5th International Conference on Experimental Fluid Mechanics ICEFM 2018 Munich
Munich, Germany, July 2-4, 2018

Drag reduction of squared-back body using continuous jets differently positioned on the rear base

Juan José Cerutti[1], **Costantino Sardu**[1], **Gaetano Iuso**[1*]

[1] Politecnico di Torino, Dimeas, Torino, Italy

[*] gaetano.iuso@polito.it

Abstract

Drag sensitivity of a square-back rear bluff body was experimentally investigated due to the effects continuous-blowing slots of limited sizes on the rear edges. Different forcing configurations were considered varying the jet velocity, the geometry and position of the slots. The drag was directly measured using a load cell. Mean and fluctuating pressure distributions were measured around the body and analyzed to interpret the drag reduction under the effect of the forcing, consequence of the wake modification. The results points to the bottom part of the rear base as the more effective for the drag reduction as well as the combination lower-lateral blowing configurations. The effect of blowing modifies considerably the wake structure according to the position of the injection slit and blowing velocity. Significant modifications in both spectra and cross-spectra of the pressure fluctuations allows possible interpretations of the wake behavior. The spectral analysis of pressure fluctuations near the bottom and the center of the rear base evidences high energy around St=0.13 corresponding to the typical vortex shedding, particularly intense in the case of unforced flow. Forcing the wake the shedding appears to be attenuated and positioned at slightly different frequency. A weak pumping of the wake is also evidenced. The cross-spectra between signals closer to the upper and lower edges evidence significant coherence around the shedding frequency for the non controlled configurations, and reduced for some of the controlled cases.

1 Introduction

The aerodynamic drag reduction (DR) of vehicles has become one of the major arguments in car design, since it can be translated in reduced gas emission for engine vehicles or extended range for electric ones. A particular kind of vehicle are the vans with square-back geometry who maximizes the internal volume and allows easy access. At the same time, these bodies present a large separated flow region causing high aerodynamic drag. Many papers in the literature are focused on the analysis of the wake structures of this kind of bodies. Rouméas et al. (2009) and Lee and Choi (2009) studied the mean behavior of the wake, and found that the near wake is characterized by a toroidal vortex structure, parallel to the rear base, and two streamwise vortexes that trail away from the model. Grandemange et al. (2013) and Volpe et al. (2015) highlighted relevant results of the wakes dynamics. These authors identify three phenomena that may occur for a squared back bluff body: a pumping mode due to the oscillation of the recirculating bubble for which the pressure distribution on the rear base fluctuates at low frequencies around St=0.05; a von Karman mode, characterized by the vortex shedding over the trailing edges at around St=0.12 and finally a bi-stability phenomenon. This last consist in the apparently random switching of the center of pressure on the rear base between two symmetrical positions, associated to a hairpin vortex structure as shown by Pavia et al. (2017). The manipulation of the wake structure aimed at the DR can be achieved through passive (PFC) and active (AFC) flow control techniques. The passive techniques were the first aerodynamic devices considered for the reduction of the base drag, reaching values up to 40% of DR as shown by Choi et al. (2014). Nevertheless, these techniques showed important limitations when considering homologation and utility of the vehicle. The AFC technique uses external energy to modify the natural flow evolution to obtain DR. In the literature is present an abundance of studies centered on the application of such forcing. As an example, some of the most relevant techniques were described in Cattafesta and Sheplak (2011). One of the most important advantage of the AFC is related with the possibility of tuning the control parameters according with the running condition of the vehicle. Moreover, AFC allows DR without the substantial

modification of the geometry of the vehicle, as shown by Manosalvas-Kjono et al. (2017). These last authors applied continuous-blowing jets device on a heavy truck model obtaining 19% of drag reduction through CFD analysis. In addition, McNally et al. (2015) studied micro-jets on the rear edges of a Honda simplified body and achieved a 3% of drag reduction. Sardu (2015) propose a square-back van model with an AFC technique based on continuous jets blowing through four independent rectangular slits positioned on the edges of the rear part. The wind tunnel and CFD results showed a maximum DR of 13% according with appropriate combinations of jets injection and forcing strength V_j/V_∞. In this paper the sensitivity of the DR of the same model tested by Sardu (2015) is investigated considering only partial openings of the jet slits, appropriate locations and different combinations of the active slits. The drag variations are highlighted by means of direct measurements using a load cell. Pressure distributions on the rear base will be studied through mean and fluctuating pressure measurements. Spectra and cross-spectra of the pressure fluctuations are evaluated from sensors positioned on the rear base in order to interpret the wake response to the forcing.

2 Experimental Setup

The experiment was carried out in the open-loop subsonic wind tunnel of the Modesto Panetti aerodynamic lab of the Politecnico di Torino. The test section width and height are respectively equal to 1100 mm and 900 mm. The length of it is equal to 6000 mm and a maximum speed of 12 m/s can be obtained. A rectangular suction slot is positioned upstream the model to reduce the boundary layer on the wind tunnel´s floor. In figure 1a is shown a sketch of the wind tunnel with the model and its support. The tests were performed for an undisturbed speed equal to 9 m/s to which corresponds a Reynolds number based on the model length $Re_L = 4.5x10^5$. A grid was settled between the end of the convergent and the test section entrance to fully develop turbulence in the test section. Hot-wire measurements in the free stream evidenced a turbulence level equal to 4% at the model´s position. The drag is directly measured through a load cell

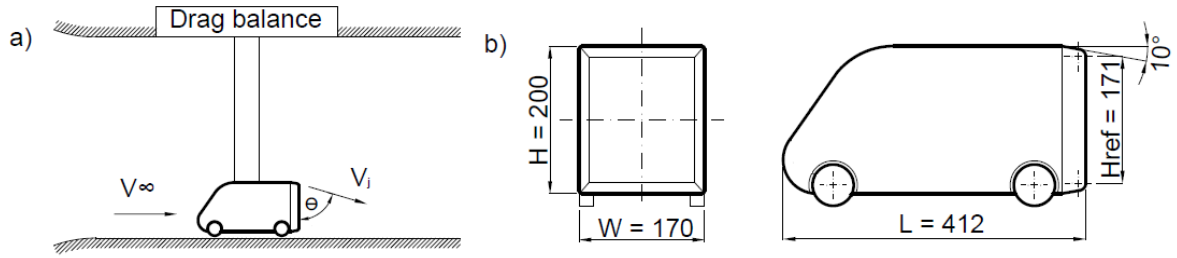

Figure 1: Wind tunnel sketch (a) and model's characteristic dimensions in millimeters (b).

mounted externally to the test section using a leverage as shown in figure 1a. A hull covers the leverage expose to the flow in order to avoid measurement contamination. The model´s scale correspond to 1:10 and its shape was based on a realistic utility van. The characteristic sizes are represented in figure 1b. The model fits inside a pressure transducer Scanivalve ZOC33 with 64 pressure taps distributed over the surface that measures the mean pressure distribution. Moreover, 16 electret capacitive microphone capsules, calibrated against a Bruel & Kjaer microphone, were distributed on the rear part to measure the pressure fluctuations. In figure 2a are shown the relevant microphones considered for this analysis, identified by their number (6, 8 and 16). Furthermore, the model is equipped with four slits of 1 mm thick along the four edges of the rear base devoted for the forcing. The full extension jets on the four edges are shown in red on figure 2a. The jets orientation and extension of the slot can be varied, reducing the size of the original slots as shown of figure 2b. An optimal blowing angle of $\Theta = 65°$was selected based on a previous CFD analysis. Moreover the strength of the forcing can be varied trough the mass flow rate variation measured with three flow meters. The data from the microphones was sampled at 10kHz for 15s through a NI cDaq 9178 chassis with NI 9215 A/D converter modules having a resolution of 16 bit. The sampled data was logged in a PC with a LabView in-house software. The measurements from the load cell were sampled with the same hardware at 1kHz and for 240s. The pressure transducer readings were directly sent to the computer via LAN connection sampling at 40Hz for 240s. The long sampling time is due to the need of obtaining statistical convergence of the mean values, because of the high unsteadiness of the wake flow. The post processing of the data includes the noise canceling of the microphones signals, as described by Sardu et al. (2016).

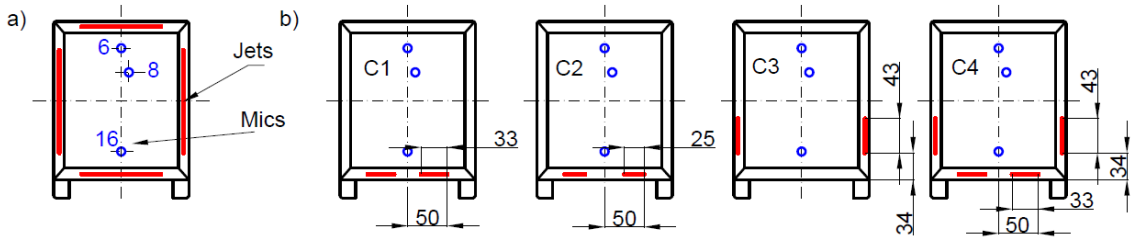

Figure 2: Full dimension jets and microphones on the model's back (a) and different jet configurations (b).

3 Results and discussion

The configurations showed in figure 2b were tested for different blowing speeds ratio V_j/V_∞ varied from 0 to 1.5. The DR as a function of V_j/V_∞ are displayed in figure 3.

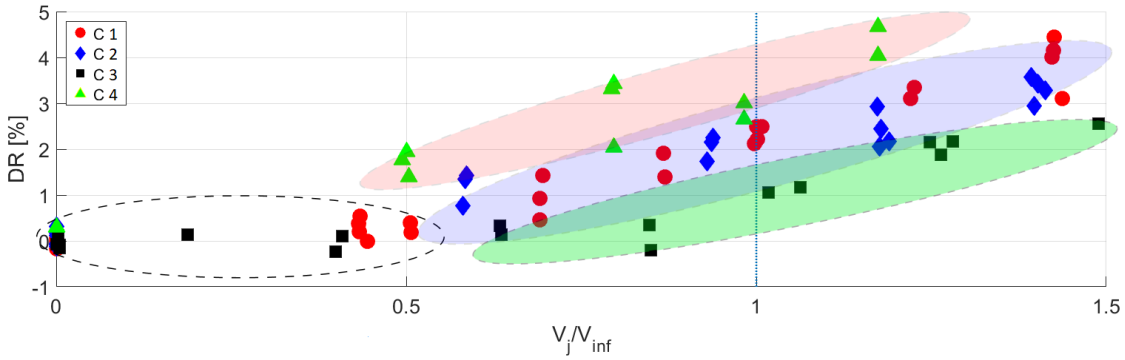

Figure 3: Drag reduction vs. blowing speed ratio for the different configurations.

The drag coefficient for the uncontrolled case, considered as reference, was equal to $C_D = 0.480 \pm 0.006$. The accuracy for each result was obtained considering the propagation error analysis in each respective chain of measurement, according to Moffat (1982). As can be seen from figure 3, if the forcing V_j/V_∞ is below 0.5 all the forced configurations are practically irrelevant, presenting around null DR. This is the evidence of a weak interaction wake-jets. When the velocity ratio is greater than 0.5 then significant effects are highlighted according to the injection arrangements. The configuration C3 is the less efficient, showing anyway increasing DR as V_j/V_∞ increases, reaching DR =2.5% for V_j/V_∞= 1.5. Configurations C1 and C2 exhibit almost the same behavior but better than that of forcing C3 giving rise to a maximum DR around 4.5% for V_j/V_∞ = 1.4. The combination of lateral and lower jet injection (C4) is clearly the most effective in the whole range of velocity ratio V_j/V_∞ reaching the maximum DR of about 5% for V_j/V_∞=1.2. It is interesting to highlight that even though the lateral forcing alone is not so effective, when it is coupled with the lower jet the wake-jet interaction results in a more favorable DR. Mean base pressure distributions in terms of pressure coefficient are reported in figure 4a in terms of color maps for the natural and controlled cases for V_j/V_∞ =1. The pressure distributions for the natural flow, C1 and C2 forced configurations exhibit common features. Nevertheless, differences are highlighted in terms of extensions and strength of low-pressure regions for the controlled cases. In configuration C1, and more pronounced in C2, pressure recovery is present and associated to a more extended higher-pressure regions. Configuration C3 evidences pressure distribution completely different respect to the two previous ones that penalizes the DR. Configuration C4 give rises to a flow organization that resemble those corresponding to C1 and C2. In particular, higher levels of pressure recovery in average involve the models base originating the highest DR as evidenced by the results of figure 3. The color maps of the pressure coefficient root mean square (RMS) distributions are displayed in figure 4b. Higher level of unsteadiness respect to the natural flow for all controlled cases are present. The distributions related to C1 and C2 are very similar to each other, as for the mean values represented in figure 4a, showing an almost uniform distribution. Configuration C3 appears to originate the highest unsteadiness on the base of the model, probably responsible of the lower drag reduction obtained. The configuration of combine jets C4 modifies considerably the distribution evidencing a concentration of

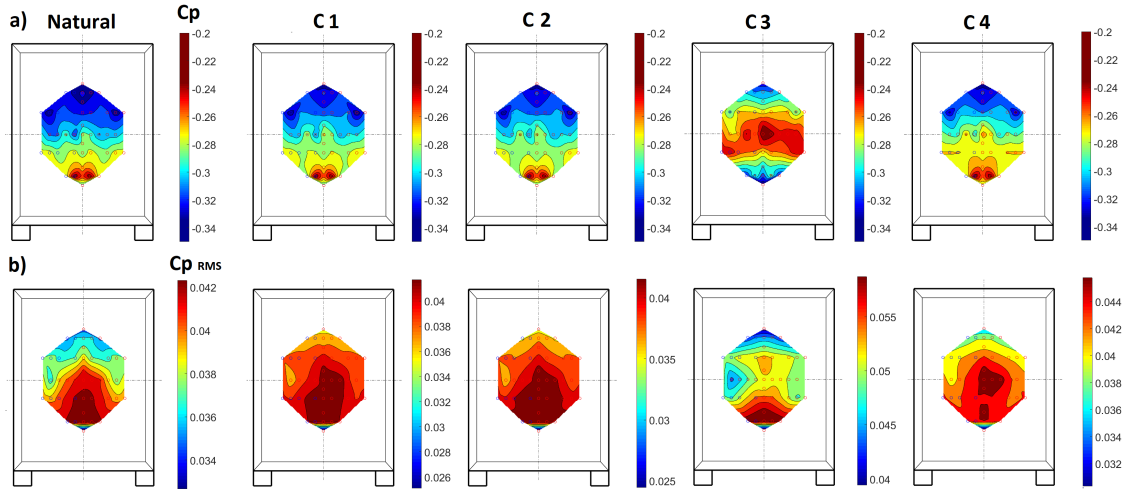

Figure 4: Mean (a) and RMS (b) pressure coefficient distribution on the rear base for natural and controlled cases at $V_j/V_\infty = 1$.

the unsteadiness centered of the rear base. Spectra and cross-spectra for the natural and forced cases are shown in figure 5. In particular, in figure 5a and 5c are displayed the spectra for the microphones 16 and 8 respectively. In figure 5b and 5d the cross-spectra power in terms of coherence and phase are presented, analyzing the signal of the cited couple of microphones. In the label of the spectra the p'_{RMS} values for each configuration are also shown. The spectra are limited at $100Hz$ since the possible aerodynamic effects are contained in this range and beyond it some spurious effects of the test (as fan rotation and structural vibrations) appear. Despite this consideration, in the range of frequency showed some mechanical spurious contributions are still present. As can be observed for both spectra, the natural case exhibit a peak of energy at $6.7Hz$ in correspondence of a Strouhal number $St = f * H_{ref}/V_{inf} = 0.13$. This is the typical value representing the shedding phenomena of the unsteady wake behavior of bluff bodies, found also by several authors as Volpe et al. (2015), Grandemange et al. (2013) and Pavia et al. (2017). In addition a weak evidence of a possible pumping mode is also present at very low frequency around $1.8Hz$ corresponding to $St = 0.034$. The forced configurations exhibit the energy concentration at a slightly lower Strouhal number value and in more or less attenuated way. The general behavior of all spectra showed in figure 5a highlight, for the frequencies above the peak, the collapse of the curves with no substantial differences between them. Below the shedding peak a modification of the energy distributions is evidenced. In particular the configurations including lower jets (C1 and C2) are characterized in average by less energy respect to the natural case. The lateral injection alone (C3) and coupled with the lower one (C4) behave similarly up to $f = 3Hz$ while for $f > 3Hz$ the configuration C3 shows the lowest energy levels. The forced configuration C4 shows reduction of energy around the shedding peak respect to the natural case other than the lowest frequency at $5Hz$ for the shedding mode. In regard to the p'_{RMS} values showed in the label of figure 5a, all controlled configurations shown a reduction of the overall energy comparing with the natural case. Configurations C1 and C2 exhibit the same value of p'_{RMS} that lead to a reduction of 6.3% respect to the uncontrolled configuration. Configuration C4 presents the maximum DR value, agreeing with a reduction of pressure fluctuations of 4.6%. The highest p'_{RMS} reduction equal to 9.3% is associated to configuration C3. The spectra of the microphone 8 (figure 5c) display behaviors not significantly different respect to the results of figure 5a. For the natural case the shedding phenomena is well clear and centered at the same Strouhal number ($St = 0.13$) while the possible pumping mode is positioned at slightly higher value ($St = 0.042$). The values of this presumable low frequency unsteadiness are very close those evidenced by Grandemange et al. (2013) and Volpe et al. (2015). For thee forced configuration the shedding is present and positioned at frequencies slightly different to those observed for microphone 16. Particularly different is the behavior of the lateral forcing C3. In fact it shows higher energy content respect to all the others cases showing a double peak of energy centered around $4Hz$ and $7Hz$ respectively. Particularly high is the amount of energy for configuration C3 in the low frequency range up to $4Hz$. Respect to the natural case, the p'_{RMS} for C3 grows up of 36%. Only configuration C2 shows reduction of p'_{RMS} equal to 5.4%. The optimal drag reduction case C4 also exhibits increasing of fluctuations respect to the natural case of about 12%. It can be observed, as expected, that also for this microphone position the lateral jets acting singularly introduce a large amount of

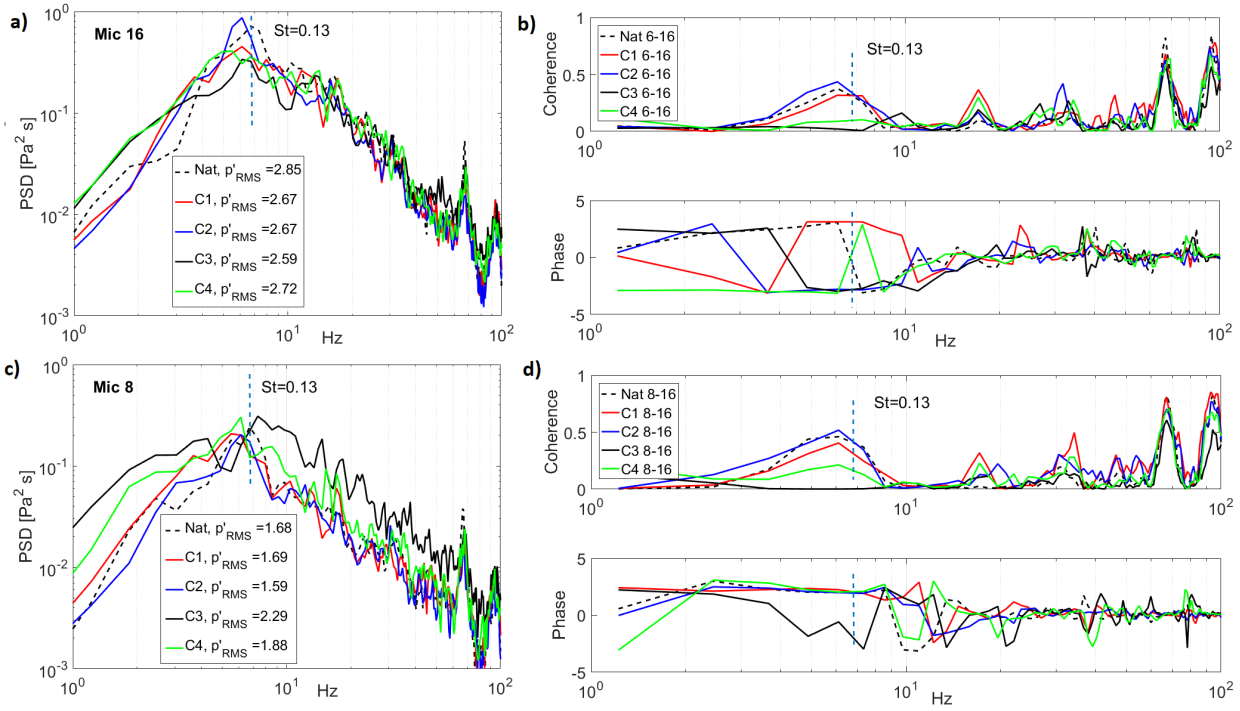

Figure 5: Spectra of microphone 16 (a), Cross-spectra of microphones 6 and 16 (b), spectra of microphone 8 (c), Cross-spectra of microphones 8 and 16 (c).

fluctuations in the wake but when they are coupled with the lower ones the unsteadiness reduce considerably. It has to be remark that it is possible to modify the dynamic of the wake´s structure using appropriately the base jets by tuning the strength and the combination of them. For all the forced configurations, it is evident from the results of figure 5a and 5c that the supposed pumping phenomenon disappear, probably due a weakening effect of the forcing. Due to the huge unsteadiness of the flow the results are highly dependent on the location of microphones. The results of the cross analysis in terms of coherence and phase as a function of the frequency are shown in figure 5b for microphones 6-16 and in figure 5d for microphones 8-16. As can be seen for both couple microphones the peaks of coherence are around $St = 0.13$ found for the spectral analysis. For the coherence related to microphones 6-16 (figure 5b), the higher levels of coherence are observed for the natural flow and for C1 and C2 forced cases. Furthermore in correspondence of these peaks of coherence the phase between the two signals shift between $\pm\pi$. Coherence and phase show that the shedding in this cases is mostly due to the regular and alternate top and bottom edges' shear layer separation, corresponding with the von Karman mode. The configurations C3 and C4 clearly exhibit loss of coherence, especially the first one for which the level of coherence is almost zero. Moreover, the phase equal to π is still present between the two pressure fluctuations from the top and bottom of the model, and this is again the evidence of the alternate shedding present in the wake. These two last configurations of forcing that involve the vertical slots indicate that the lateral jets are able to modify the shedding, weakening or cancelling the correlation of the rolling layers separating from the top and bottom edges. The mechanism underlying the loss of coherence is not easy to explain. Probably, the responsible are the smaller scales structures injected from the jets into the wake that weaken the flow organization of the large shear layers during their phase of formation, rolling up and detachment from the edges. For frequencies higher than $10Hz$ all the curves of the coherence and phase assume a similar behavior also evidenced in the spectra. This behavior is probably due to different smaller scales interactions that behaves approximately in the same way for the natural and the forced cases. It has to be remarked that peaks of coherence in correspondence of $66Hz$ and $94Hz$ are spurious contributions due to the vibrations of the lateral wall of the wind tunnel. For the Cross-spectra 8-16 (figure 5d), very similar results to the previous analysis were found. In fact the coherence follows almost the same trend in all the cases, except for C4 configuration for which the coherence is higher respect to coherence between the signals 6-16. The phase shows slightly lower values respect to π that can be associated to the different relative position of the microphones. Furthermore, the phase for C3 forcing shows more irregularity respect to the 6-16 case. From the cross-correlation previous analysis it evident that

even though each spectrum pertaining to each microphone exhibit peaks of energy approximately for the same shedding frequency, the correlation between the two signal can be completely lost.

4 Conclusion

The drag variation of the model shows an important dependence to the forcing configuration tested other than the forcing strength. The comparison between lower and lateral blowing slots evidences that the lower part is the more effective in terms of drag reduction. Moreover, it is shown that the lateral jets are weakly effective if injected singularly but combined with the lower one originates the maximum drag reduction of the order of 5%. The distribution of base pressure shows the changes on the topology of the near wake and an increasing of base pressure for all controlled cases responsible of the reduced drag. The statistical values of the pressure fluctuations give evidence of more global attenuations of the wake unsteadiness in the cases of the forcing. Different modifications on the spectra are induced according with the forcing configuration. The shedding mode is highlighted and it is shown its high sensitivity to the forcing. A weak evidence ascribable to a possible pumping phenomenon is also noticed. Finally, the lateral forcing shows high capability in de-correlating the coherence of the shear layers when combined with the lower injection.

Acknowledgements

To the "Modesto Panetti" Aerodynamic lab's personnel, Mr. Marco Cannata and Mr. Marco Grivet

References

Cattafesta L and Sheplak M (2011) Actuators for active flow control. *Annual Review of Fluid Mechanics* 43:247–272

Choi H, Lee J, and Park H (2014) Aerodynamics of heavy vehicles. *Annual Review of Fluid Mechanics* 46:441–468

Grandemange M, Gohlke M, and Cadot O (2013) Turbulent wake past a three-dimensional blunt body. part 1. global modes and bi-stability. *Journal of Fluid Mechanics* 722:51–58

Lee J and Choi H (2009) Large eddy simulation of flow over a three-dimensional model vehicle. *Sixth International Symposium on Turbulence and Shear Flow Phenomena. June 22-24. Seoul, Korea*

Manosalvas-Kjono D, Economon T, Othmer C, and Jameson A (2017) Computations of active flow control for heavy vehicle drag reduction. *35th AIAA Applied Aerodynamics Conference*

McNally J, Fernandez E, Robertson G, Kumar R, Taira K, Alvi F, Yamaguchi Y, and Murayama K (2015) Drag reduction on a flat-back ground vehicle with active flow control. *Journal of Wind Engineering and Industrial Aerodynamics* 145:292–303

Moffat RJ (1982) Contributions to the theory of single-sample uncertainty analysis. *Journal of Fluid Engineering* 104(2):58–250

Pavia G, Passmore M, and Sardu C (2017) Evolution of the bistable wake of a squareback automotive shape. *Experiments in Fluids*

Rouméas M, Gilliéron P, and Kourta A (2009) Analysis and control of the near-wake flow over a square-back geometry. *Computers and Fluids* 38:60–70

Sardu C (2015) Drag reduction on a simplified 3d bluff body. *European Drag Reduction and Flow Control Meeting, EDRFCM. March 23-26. Cambridge, UK*

Sardu C, Lasagna D, and Iuso G (2016) Noise filtering for wall-pressure fluctuations in measurements around a cylinder with laminar and turbulent flow separation. *Journal of Fluid Engineering* 138

Volpe R, Devinant P, and Kourta A (2015) Experimental characterization of the unsteady natural wake of the fullscale square back ahmed body: flow bistability and spectral analysis. *Exp Fluids* May:56–99